Received 31 May 2023; revised 25 July 2023; accepted 6 August 2023. Date of publication 10 August 2023; date of current version 28 August 2023.

Digital Object Identifier 10.1109/OJCOMS.2023.3304022

Mission-Critical Connectivity Enhanced by IAB in Beyond 5G: Interplay of Sidelink, Directional Unicasting, and Multicasting

OLGA CHUKHNO [1,2] (Member, IEEE), NADEZDA CHUKHNO [3] (Member, IEEE), SARA PIZZI [1,2] (Member, IEEE), ANTONINO ORSINO [4], HELKA-LIINA MÄÄTTÄNEN [4], JOHAN TORSNER [4], ANTONELLA MOLINARO [1,2], ANTONIO IERA [2,5] (Senior Member, IEEE), AND GIUSEPPE ARANITI [1,2] (Senior Member, IEEE)

[1] DIIES Department, University Mediterranea of Reggio Calabria, 89124 Reggio Calabria, Italy
[2] Department of Information and Communication Technology, CNIT, 43124 Parma, Italy
[3] Faculty of Information Technology and Communication Sciences, Tampere University, 33014 Tampere, Finland
[4] Ericsson Research, 02420 Jorvas, Finland
[5] DIIES Department, University of Calabria, 87036 Arcavacata, Italy

CORRESPONDING AUTHOR: N. CHUKHNO (e-mail: nadezda.chukhno@tuni.fi)

This work was supported by the European Union's Horizon 2020 Research and Innovation programme under the Marie Skłodowska Curie Grant under Agreement 813278 (A-WEAR: A Network for Dynamic Wearable Applications With Privacy Constraints, http://www.a-wear.eu/).

ABSTRACT Guaranteeing operational connectivity in emergency situations by means of prompt on-demand network re-configuration is crucial to carry out effective public protection and disaster relief actions. This article analyzes network configuration options enhanced by the integrated access backhaul (IAB) feature for 5G-Advanced and beyond mission-critical services. We specifically aim to investigate the possible interplay of sidelink communications, directional unicast transmissions, and multicasting. To this end, we offer a practical methodology based on a fluid model approximation to capture the time dynamics of mission-critical services in their transient phase. Simulation results show that the interplay of multicasting, unicasting, and sidelink is a highly effective solution for mission-critical communications. In contrast, standalone unicast, multicast, and sidelink transmissions are unable to support such services. A further emerging aspect is that, in a mixed unicast-multicast-sidelink configuration, optimal results are obtained when multicast exploits most of the available resources, specifically more than 70%.

INDEX TERMS 5G-Advanced, wireless communications, multicast, unicast, NR sidelink, IAB, mission-critical services, fluid approximation.

I. INTRODUCTION

IN EMERGENCY situations, caused by natural or man-made events, telecommunication networks could be severely affected and no longer available, whereas guaranteeing operational connectivity would be essential to carry out effective public protection and rescue actions. To fulfill the connectivity requirement of the current fifth generation (5G) network, emergency scenarios call for a prompt on-demand network re-configuration, which may also benefit from ad-hoc deployed cells-on-wheels and/or cells-on-wings base stations (BSs), offering great flexibility in establishing temporary networks.

Recently, mission-critical public safety communications have shifted from voice-only to broadband low-latency services. Exemplary use cases include the remote operation of drones and robotics, the use of haptic sensors in fire-fighters' personal protective equipment for faster and safer search-and-rescue in a burning building with heavy smoke, and connected ambulance with remote assistance from a medical specialist [1].

Furthermore, the nature of public safety mission-critical communications is mostly group-oriented [2]. Indeed, first responders typically work in groups and need to coordinate their operations. Thus, providing the same content

to a set of users through multicasting represents a means of achieving effective group communications, in terms of both network resource utilization and quality of service provision.

Driven by the rising demand for reliable, responsive, and broadband connectivity to improve safety, the 3rd Generation Partnership Project (3GPP) has started since 2016 to include functionalities for the delivery of mission-critical applications over mobile cellular networks [3]. Among the solutions that can be effectively exploited in public safety scenarios, currently included in the 5G New Radio (NR) standard, is the use of the millimeter wave (mmWave) spectrum to improve coverage. MmWaves bring the benefit of increasing the signal strength for target users, thus providing Gbps communications by implementing proper beamforming techniques [4].

A key role in mission-critical communications delivery will also be played by *integrated access backhaul (IAB)* [5], which combines wireless backhauling and access capabilities by means of multi-hop network relaying. As a result, IAB enables extended coverage, improved network capacity, and enhanced reliability, making it particularly suitable for mission-critical scenarios where continuous and robust connectivity is vital. Furthermore, *sidelink (SL)* transmissions enable proximity communications among neighboring devices to provide coverage in areas where the network infrastructure is unavailable or damaged. Finally, 5G will support group communications via the *multicast and broadcast services (MBS)* system architecture [6], delivering real-time updates, emergency alerts, live video streaming, and other group-oriented services with improved efficiency and scalability.

In this article, we take as a reference a mission-critical scenario in which the BS is temporarily blocked/unavailable. Thus, IAB nodes need to be used to enhance coverage and provide service to all users in the area of interest with the required content. In order to take advantage of all the above-discussed solutions to cope with the emergency, we investigate the interplay of sidelink communications, directional unicast transmissions, and multicasting and provide a tool for analyzing the performance of all possible network configuration options. Specifically, we mathematically characterize the system behavior through a fluid-based model that captures the time dynamics of arrival/service/departure processes in their transient phase, which is the inherent nature of mission-critical services. The proposed model works as a means for the emergency management team to determine the network configuration option that better suits the mission-critical situation being under control.

The remainder of this work is organized as follows. Section II presents the background of the work and the main related work in the field. In Section III, the contributions of the work are detailed. Section IV introduces the system model, while in Section V, we present the proposed model for network configuration option analysis. Simulative results are discussed in Section VI. Finally, Section VII concludes this work.

II. BACKGROUND AND RELATED WORK

A large body of literature has sought to provide techniques to mitigate the inherent limitations of current communication systems in meeting mission-critical service requirements. Along this line, a reliability analysis of mmWave access has been provided in [7], where a comprehensive methodology to model the softwarized 5G radio access network (RAN) managing high-rate mission-critical traffic has been developed. The framework also analyzes the corresponding impact of critical session transfers on other user sessions. The authors state that both high-rate critical sessions and the high velocity of the target user lead to a significant degradation of the other user sessions, which can be mitigated by proper usage of multi-connectivity in mmWave networks and by splitting the fallback traffic across multiple microwave technologies.

A different approach to reliability support in 5G networks has been reported in [8], wherein the Raft protocol has been used to achieve an ultra-reliable and low-latency consensus for mission-critical distributed Industrial Internet of Things (IIoT). Within this study, the "reliability gain" concept has been proposed to mathematically characterize the relationship between consensus reliability and communication link reliability. It has also been highlighted that the consensus latency is contradictory to reliability.

Decentralized event-triggered scheduling and fusion of information for mission-critical Internet of Things (IoT) sensors have been designed in [9]. Instead of a high-complexity Kalman filter, a fixed gain remote state estimator and a novel algorithm for the design of the fixed filtering gain via minimizing the remote state estimation mean square error have been offered when considering perfect symbol level synchronization. More recently, in [10], the study in [9] has been extended by taking into account more complex remote state estimation with asynchronous mission-critical IoT sensors.

An analysis of mission-critical service under a different perspective has been proposed in [11], where the impact of the device- and application-related parameters on the latency and the reliability performance of public safety applications has been examined. Similarly, the effects of heterogeneous user and device mobility on the performance of mission-critical machine-type communications within a multi-connectivity 5G network have been examined in [12]. According to [12], alternative connectivity options, such as device-to-device (D2D) links and drone-based access, may contribute to fulfilling the requirements of mission-critical machine-type communication applications.

To this end, a considerable body of literature has also been focused on using D2D communication for mission-critical applications to improve cellular network coverage. For example, in [13], edge-based mission-critical IoT applications reckon on collaborative D2D links between the IoT devices

TABLE 1. Summary of related works relevant to mission-critical scenarios.

Work	Task	Approach	Technologies	Limitations
		Cellular connectivity		
[7]	End-to-end reliability of mission-critical traffic	Mathematical framework	Network softwarization, multi-connectivity	No multicast and D2D transmission options, no IAB
[8]	Ultra-reliable and low latency consensus	Analysis of consensus reliability in distributed IIoT systems with Raft	Distributed IIoT	
[9], [10]	Remote state estimation stability of system with synchronous/asynchronous sensors	Lyapunov optimization	5G wireless networks	
[11]	Performance evaluation of wearable-based mission-critical applications, latency and reliability trade-off mechanisms in mission-critical applications	Network simulation using ns-3 LTE LENA module	Cellular connectivity	
		D2D		
[12]	Study the impact of heterogeneous mobility on connection availability and reliability	Heterogeneous multi-connectivity approach, simulation	Multi-connectivity 5G network, D2D, UAV, cellular	No multicast and unicast transmission options, no IAB
[13]	How D2D-based transmissions may facilitate the deployment of cooperative IoT services at the network edge	Simulation-based study	5G, edge, D2D	
[14], [15]	Enhancement of cellular networks with D2D	Cluster formation-based mathematical framework	Cellular connectivity, D2D	
[16]	Propose self-organized use case of URLLC-constrained D2D communication	Theoretical results	Cellular connectivity, IIOT, D2D	
[17]	Improve end-to-end latency and energy efficiency when using D2D communication	Simulation-based study	5G NR, D2D	
		Multicasting		
[1]	Overview of the 3GPP NR features in supporting public safety mission-critical communications	Overview	Cellular connectivity, multicasting	No D2D and unicast transmission options, no IAB
[18]	SINR model	Closed-form formula of the SINR	Cellular network, MBSFN	
[19], [20]	Robust transceiver design	Dynamic clustering, optimization problem	MBSFN, SC-PTM	
[21]	Efficient use of radio resources	Simulation comparison of MBSFN, SC-PTM, unicast transmission modes	MBSFN, SC-PTM, unicasting	
		IAB		
[1]	Overview of the 3GPP NR features in supporting mission-critical communications	Overview	Cellular connectivity, IAB	No D2D and multicast transmission options
[22]	Potential and research challenges for IAB	End-to-end system-level simulations	5G mmWave, IAB	
[23]	Leveraging UAV mobility to serve moving users and improve system performance	Performance dynamics and optimization	5G mmWave, IAB	
[24]	Fast and reliable connectivity to enhance situational awareness and operational efficiency	Reinforcement learning	UAV-based IAB system, 5G NR	
[25]	Improved coverage	Simulation-based study	LTE, heterogeneous-network, UAV BSs	
[26]	Resilient public safety	Simulation-based study	UAV-assisted 5G cellular	
		Interplay of sidelink, directional unicasting, and multicasting as "edge" IAB access		
Our work	Analysis of network configuration options enhanced by IAB	Mathematical framework, closed-form solution for the number of users involved in a mission-critical situation	mmWave, IAB, unicast, multicast, D2D	

in the presence of mobility. Similarly, in [14], [15], user clustering and D2D communications among the closest users have been considered as effective strategies to connect users and preserve their energy in the disaster region. In [16], the authors developed a cognitive approach to meet the required reliability and throughput in D2D transmissions while taking into account the interference constraints imposed by primary and inter-cell users. In [17], improvements in end-to-end latency and energy efficiency when using NR sidelink communication for mission-critical scenarios compared to LTE, LTE sidelink, and NR transmissions have been demonstrated.

Similarly, several studies on the exploitation of multicasting for mission-critical scenarios have been conducted, including but not limited to [1], [18], [19], [20], where different clustering methods and propagation models have been developed. In [21], a comparison among multicast broadcast single frequency network (MBSFN), single-cell point-to-multipoint (SC-PTM), and unicast transmission modes in mission-critical use cases has been presented from a resource use perspective. As per the results, SC-PTM might be considered as the best option for locally restricted and small-scale emergencies, whereas MBSFN might be preferable for emergencies during massive events or those affecting a large region.

A further feature of 5G NR that can be used for mission-critical applications is the IAB [22], [23]. IAB can also be used for its potential to wirelessly connect several unmanned aerial vehicles carrying BS (UAV-BS) and easily integrate them into an existing mobile network. In [24], a UAV-BS has been integrated into the mobile network using the 5G IAB technology to provide temporary coverage in a disaster area. Thanks to UAVs' excellent mobility and high flexibility, UAV-BSs are supposed to bring fast connectivity for mission-critical communications [25], [26].

A summary of the discussed related works is provided in Table 1, highlighting that mission-critical communications do not consider the possibility of exploiting different transmission modes. Such options are necessary to improve the

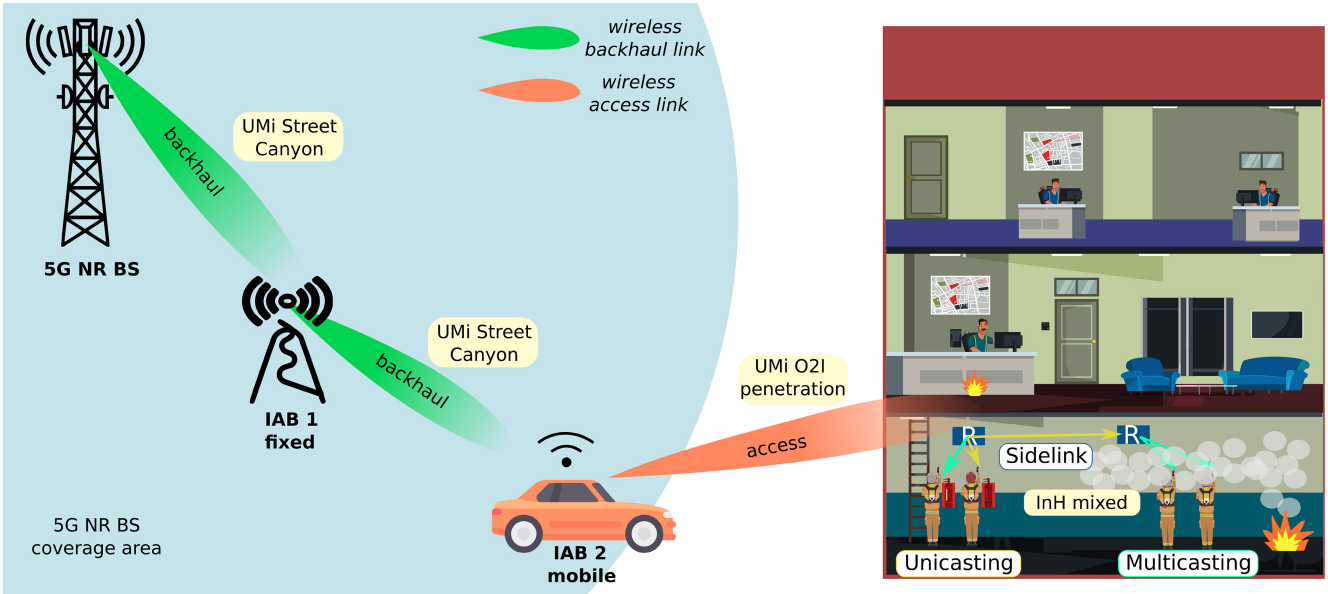

FIGURE 1. System illustration.

overall system reliability, flexibility, and coverage, especially in emergency situations.

Although the revised studies have gone some way towards enhancing the reliability, latency, security, and other crucial aspects of mission-critical services by exploiting approaches that facilitate cellular connectivity, no works have focused on providing an effective tool that can guide the selection of the network configuration to promptly and efficiently provide coverage in areas affected by critical situations. In this work, we fill this gap by mathematically characterizing the time dynamics of mission-critical services in their transient phase delivered by means of the possible interplay of unicast, multicast, and NR sidelink transmissions.

III. FOCUS AND CONTRIBUTIONS OF THIS WORK

We consider a mission-critical scenario with multiple users coexisting in an indoor, outdoor, or mixed indoor/outdoor environment. An illustrative example of the scenario under analysis is shown in Fig. 1. We assume that the 5G NR BS is temporarily blocked or unavailable, thus, an IAB node needs to be activated to provide coverage to users. A set of IAB nodes are located within the area of interest, and their positions are chosen in such a way as to provide coverage to a high number of users. We underline that IAB node positioning is a problem itself, as discussed in [27], which is not the focus of our work.

The connection from the BS to the user may go through a chain of IAB nodes, i.e., by multi-hopping. Further, IAB nodes may be fixed nodes (i.e., cell tower BSs, rooftop-mounted UAVs, static vehicles) and/or on-demand deployed mobile nodes (i.e., flying UAVs, moving vehicular devices).[1]

1. 3GPP is actively working on Release 18, enhancing the NR IAB solution, with a specific focus on scenarios where mobile-IAB nodes are mounted on vehicles [28].

In our study, we split the BS-to-user connection into *(i)* the backhaul connection from the BS to the "edge" IAB node and *(ii)* the access connection from the "edge" IAB node to the users. Specifically, we focus on the access connection under the assumption that the backhaul connection from the BS to the "edge" IAB node remains unchanged.

For the first time, this article seeks to analyze the operation of the network during emergency situations through the *interplay* of sidelink, directional unicasting, and multicasting technologies. More specifically, we investigate the following *network configuration* options for the access connection:

1) *Unicast mode.* The transmissions from the "edge" IAB node to the users are performed via simultaneous unicast transmissions.
2) *Multicast mode.* The transmissions from the "edge" IAB node to the users are performed via a single multicast transmission.
3) *Sidelink mode.* The transmissions from the "edge" IAB node to the users are performed via sidelink transmissions, i.e., a chain of transmissions.
4) *Mixed Unicast-Multicast mode.* The transmissions from the "edge" IAB node to the users are performed via both unicast and multicast transmissions.
5) *Mixed Unicast-Sidelink mode.* The transmissions from the "edge" IAB node to the users are performed via both unicast and sidelink transmissions.
6) *Mixed Multicast-Sidelink mode.* The transmissions from the "edge" IAB node to the users are performed via both multicast and sidelink transmissions.
7) *Mixed Unicast-Multicast-Sidelink mode.* The transmissions from the "edge" IAB node to the users are performed via unicast, multicast, and sidelink transmissions.

We note that, in this work, the concepts of service and delivery methods and of transmission modes are different. Specifically, we assume that all users require the same mission-critical service/content, while multicast, unicast, and sidelink transmission options for access connection can be utilized to deliver the given service/content to users.

The main contributions of our work can be summarized as follows:

- We investigate the synergies resulting from a joint usage of unicast, multicast, and sidelink transmissions, as well as their individual performance in the case of mission-critical services.
- We propose a novel analytical model based on a fluid approximation to mathematically characterize the system behavior.
- We derive the closed-form expressions for the number of users involved in a mission-critical situation and capture the temporal dynamics of arrival/departure/transition processes in their transient phase.
- We implement an extensive performance evaluation campaign to investigate the impact of the input parameters on meaningful performance metrics.
- We offer an analysis of the time-dependent behavior of user requests in their transient phases for mission-critical scenarios, that work as a means for a proper transmission configuration option.
- We demonstrate with the achieved results that the combination of multicasting, unicasting, and sidelink operations presents a remarkably effective solution for mission-critical communications. The best outcome is achieved by maximizing the utilization of multicast resources, which comprise the predominant portion (exceeding 70%) in a mixed unicast-multicast-sidelink configuration.

IV. SYSTEM MODELING

This section details the system model underlying our proposal aimed at analyzing the network configuration options in mission-critical scenarios. Notations used throughout this work are summarized in Table 2.

A. DEPLOYMENT

We consider a mixture of outdoor and indoor environments within an area of N m x M m. More specifically, the BS is located outdoors in the origin of the coordinate system, i.e., at $(0, 0, h_{\text{BS}})$, where h_{BS} is the BS height. The location of the first IAB node is fixed and set to $(x_{\text{IAB1}}, y_{\text{IAB1}}, h_{\text{IAB1}})$ outdoors, where h_{IAB1} is the height of IAB 1. By analogy, the height of IAB 2 (also known as "edge" IAB) is h_{IAB2}. It is located outdoors at d m distance far from the building placed at the reference point with coordinates $(x_{\text{R}}, y_{\text{R}}, h_{\text{EU}})$, generated according to a uniform distribution. The indoor users are uniformly distributed in a circle of radius R around the reference point.

TABLE 2. Notations used in this work.

Parameter	Definition
System model components	
$(0, 0, h_{\text{BS}})$	BS's location
h_{BS}	Height of BS, m
$(x_{\text{IAB1}}, y_{\text{IAB1}}, h_{\text{IAB1}})$	Location of IAB 1 node
h_{IAB1}	Height of IAB 1 node, m
$(x_{\text{IAB2}}, y_{\text{IAB2}}, h_{\text{IAB2}})$	Location of IAB 2 ("edge" IAB) node
h_{IAB2}	Height of IAB 2 node, m
$(x_{\text{R}}, y_{\text{R}}, h_{\text{UE}})$	Location of reference point (for user distribution)
h_{UE}	Height of users, m
R	Radius of circle within that indoor users are deployed, m
d	Distance between IAB 2 ("edge" IAB) node and reference point, m
NxM	Dimensions of area of interest, m
f_c	Carrier frequency (backhaul and access), GHz
d_{3d}	3D distance between transmitter and receiver, m
d_{2d}	2D distance between transmitter and receiver, m
$d_{\text{2D-in}}$	Minimum of two independently generated uniformly distributed variables, m
β, ζ	Propagation coefficients
$\text{PL}_{\text{b}}(d_{\text{3d}})$	Basic outdoor UMi path loss, dB
$\text{PL}_{\text{of}}(d_{\text{3d}})$	Indoor Office InH path loss, dB
PL_{tw}	Building penetration loss through the external wall, dB
PL_{in}	Inside loss dependent on the depth into the building, dB
σ_P	Standard deviation for the penetration loss in decibels
$p_L(d_{\text{2d}})$	LoS probability
$\text{SNR}(d_{\text{3d}})$	Signal-to-noise ration, linear scale
P_t	Transmit power, watt
N_0	Power spectral density of noise per 1 Hz, linear scale
W_{snr}	Available bandwidth, Hz
W	Available bandwidth, MHz
M_{I}, M_{S}	Interference and shadow fading margins, linear scale
D_0	Maximum directivity along the boresight, dBi
α	Deviating from antenna boresight, $^\circ$
θ_{hpbw}	Half-power beam width, $^\circ$
Framework components	
λ	Arrival rate of search & rescue operators, s^{-1}
θ_x	Departure rate of waiting users, s^{-1}
θ_y	Departure rate of served users, s^{-1}
θ_z	Departure rate of search & rescue operators, s^{-1}
μ_x	Transition rate from *served users* to *waiting users*, s^{-1}
C_0^u	Unicast capacity, Gbps
C_0^m	Multicast capacity, Gbps
C_0^d	Sidelink capacity, Gbps
B	Content/packet size, Mb
$x(t)$	Actual number of waiting users
$y(t)$	Actual number of served users
$z(t)$	Actual number of search & rescue operators
t	Instant time moment

B. PROPAGATION AND BLOCKAGE MODELS

The basic outdoor path loss in decibel scale at three-dimensional (3D) distance d_{3d} for urban micro (UMi) Street Canyon model in case outdoor propagation between the BS and the IAB 1, as well as between the IAB 1 and the IAB 2 (see Fig. 1) reads as in [29]:

$$\text{PL}_{\text{b}}(d_{\text{3d}})[dB] = \beta + 10\zeta \log_{10} d_{\text{3d}} + 20 \log_{10} f_c, \qquad (1)$$

where f_c is the carrier frequency in GHz, d_{3d} is the 3D distance between the transmitter and the receiver (i.e., BS-IAB 1 and IAB 1-IAB 2 distances). The coefficients β and ζ account for line-of-sight (LoS)/non-line-of-sight (nLoS) states as well as for LoS blocked and LoS non-blocked channel conditions. In detail, 3GPP recommends $\zeta = 2.1$ and $\zeta = 3.19$ for LoS and nLoS states [29], whereas the value of β depends on the carrier frequency. In non-blocked conditions for the lower part of mmWave band (i.e., $28-78$ GHz), β is 32.4 dB. The blockage attenuation in the blocked

state is added on top, resulting in an additional loss in the range of $15-25$ dB [30], [31].

We employ the UMi 3GPP path loss model considering outdoor-to-indoor (O2I) penetration loss, as described below, to model the propagation path between the outdoor transmitter (i.e., edge IAB) and the receiver (i.e., user) located inside the building. The path loss incorporating O2I building penetration loss is modeled as in [32]:

$$\mathrm{PL}(d_{3\mathrm{d}})[dB] = \mathrm{PL}_{\mathrm{b}}(d_{3\mathrm{d}}) + \mathrm{PL}_{\mathrm{tw}} + \mathrm{PL}_{\mathrm{in}} + \mathcal{N}\left(0, \sigma_P^2\right), \quad (2)$$

where $\mathrm{PL}_{\mathrm{b}}(d_{3\mathrm{d}})$ is the basic outdoor UMi path loss as per (1), $\mathrm{PL}_{\mathrm{tw}}$ is the building penetration loss through the external wall, $\mathrm{PL}_{\mathrm{in}}$ is the inside loss dependent on the depth into the building, and σ_P is the standard deviation for the penetration loss.

Path loss through external wall, $\mathrm{PL}_{\mathrm{tw}}$, in the case of low-loss ($\sigma_P = 4.4$ dB) and high-loss model ($\sigma_P = 6.5$ dB), respectively, is given by:

$$\mathrm{PL}_{\mathrm{tw}}[dB] = 5 - 10\log_{10}\left(0.3 \cdot 10^{\frac{-2-0.2f_c}{10}} + 0.7 \cdot 10^{\frac{-5-4f_c}{10}}\right), \quad (3)$$

$$\mathrm{PL}_{\mathrm{tw}}[dB] = 5 - 10\log_{10}\left(0.7 \cdot 10^{\frac{-23-0.3f_c}{10}} + 0.3 \cdot 10^{\frac{-5-4f_c}{10}}\right), \quad (4)$$

while indoor loss, $\mathrm{PL}_{\mathrm{in}}$, can be calculated as follows

$$\mathrm{PL}_{\mathrm{in}} = 0.5 d_{\text{2D-in}}, \quad (5)$$

where $d_{\text{2D-in}}$ is minimum of two independently generated uniformly distributed variables between 0 and 25 m UMi-Street Canyon model:

$$d_{\text{2D-in}} \sim \min_{i=1,2} \mathcal{U}(0, 25). \quad (6)$$

The LoS probability for the two-dimensional distance $d_{2\mathrm{d}}$, $p_L(d_{2\mathrm{d}})$, is derived for UMi Street path loss model:

$$p_L(d_{2\mathrm{d}}) = \begin{cases} 1, & d_{2\mathrm{d}} \le 18\mathrm{m}, \\ \frac{18}{d_{2\mathrm{d}}} + e^{-\frac{d_{2\mathrm{d}}}{36}}\left(1 - \frac{18}{d_{2\mathrm{d}}}\right), & d_{2\mathrm{d}} > 18\mathrm{m}. \end{cases} \quad (7)$$

Further, the propagation loss in the case of indoor multi-hop relaying is assumed to follow the indoor 3GPP model (InH - office) [29]:

$$\mathrm{PL}_{\mathrm{of}}(d_{3\mathrm{d}})[dB] = \begin{cases} \beta + 17.3\log_{10} d_{3\mathrm{d}} + 20\log_{10} f_c, & \text{LoS}, \\ \beta + 31.9\log_{10} d_{3\mathrm{d}} + 20\log_{10} f_c, & \text{nLoS}. \end{cases} \quad (8)$$

Hence, for InH - office model, 3GPP suggests $\zeta = 1.73$ and $\zeta = 3.19$ for LoS and nLoS states, respectively.

In the case of Indoor - Mixed office, the LoS probability for the 2D distance, $d_{2\mathrm{d}}$, for indoor is written as:

$$p_L(d_{2\mathrm{d}}) = \begin{cases} 1, & d_{2\mathrm{d}} \le 1.2\mathrm{m}, \\ e^{-\frac{d_{2\mathrm{d}}-1.2}{4.7}}, & 1.2 < d_{2\mathrm{d}} < 6.5\mathrm{m}, \\ 0.32e^{-\frac{d_{2\mathrm{d}}-6.5}{32.6}}, & d_{2\mathrm{d}} \le 6.5\mathrm{m}. \end{cases} \quad (9)$$

The general formulation of Signal-to-Noise Ratio (SNR) is given by:

$$\mathrm{SNR}(d_{3\mathrm{d}}) = \frac{P_t D_0 \rho(\alpha)}{N_0\, W_{\mathrm{snr}}\, \mathrm{PL}(d_{3\mathrm{d}})\, M_{\mathrm{I}}\, M_{\mathrm{S}}}, \quad (10)$$

where P_t is the transmit power, N_0 is the power spectral density of noise per 1 Hz, and W_{snr} is the bandwidth in Hz, M_{I} M_{S} are interference and shadow fading margins, whereas $\mathrm{PL}(d_{3\mathrm{d}})$ represents the path loss (that depends on the environment).

C. ANTENNA MODEL

We now introduce the antenna model that is formulated as follows. The main antenna lobe is assumed to be symmetric w.r.t. the antenna boresight axis. The transmit antenna gain $G_T(\alpha)$ can then be simply provided as [33], [34]:

$$G_T(\alpha) = D_0 \rho(\alpha), \quad (11)$$

where D_0 represents the maximum directivity along the boresight, $\rho(\alpha)$ is the directivity function of the angular deviation from the boresight direction, whereas $\alpha \in [0, \pi]$. The total directivity is defined by $\rho(0) = 1$.

The function $\rho(\alpha)$ can be found as [33], [34]:

$$\rho(\alpha) = \begin{cases} 1 - \frac{\alpha}{\theta}, & \alpha \le \theta_{\mathrm{hpbw}}, \\ 0, & \text{otherwise}, \end{cases} \quad (12)$$

where θ_{hpbw} is the half-power beam width (HPBW).

D. NETWORK TRAFFIC DYNAMICS

In a mission-critical scenario, we can identify two types of nodes: victims of the situation, referred to as *users*, and *search & rescue operators*. Users need to be provided with data content by means of either a unicast/multicast transmission by the edge IAB node or by a sidelink communication with *search & rescue operators*. Users can be in one of the following two states: (i) users who are waiting to receive the content, i.e., *waiting users* and (ii) users who have already received the content, i.e., *served users*. Differently, *search & rescue operators* do not change state and work as a means for sidelink transmission.

Specifically, we assume that the following arrival/transition/departure processes influence/determine the number of nodes in the system:

(i) *Arrival process*:
- *Waiting users* are already in the system and not supposed to externally arrive into the system (no arrival process);
- *Served users* are not supposed to externally arrive into the system (no arrival process);
- *Search & rescue operators* arrive externally according to the Poisson process with the arrival rate λ.[2]

2. The Poisson process can be used to model the arrival of *search & rescue operators* into a building with, e.g., fire. In this scenario, the operators are assumed to arrive independently of each other, one by one.

(ii) *Transition process*:
- *Waiting users* can change their state to *served users* after receiving the content by means of either a unicast, multicast, or sidelink transmission from *search & rescue operators*;
- *Served users* may request the updated content and, therefore, be transformed into *waiting users* with the average rate μ_x;
- *Search & rescue operators* are not prone to transition.

(iii) *Departure process*:
- *Waiting users* depart from the system with the rate θ_x;
- *Served users* depart from the system with the rate θ_y;
- *Search & rescue operators* depart from the system with the rate θ_z.

We assume that wireless connectivity to the users via both unicast and multicast communications is provided by the "edge" IAB node, while sidelinks can be established with *search & rescue operators*. Radio resources are split among the three considered transmission modes (more insights will be given in the following section).

Unicast users equally share in time and/or frequency radio resources exploitable for unicasting. Therefore, the transition from *waiting users* to *served users* by means of unicast transmissions corresponds to:

$$C_u(t) = \frac{1}{x(t)} \frac{C_0^u}{B}, \tag{13}$$

where $x(t)$ is the actual number of *waiting users*, C_0^u is the unicast downlink capacity, whereas B represents the content size.

In the case of multicasting, users are organized in one multicast group that is assigned with all channel resources devoted to the multicast transmission. The transition from *waiting users* to *served users* by means of multicasting is, therefore, given by

$$C_m(t) = \frac{C_0^m}{B}, \tag{14}$$

where C_0^m is the multicast downlink capacity.

Finally, in the case of sidelink transmissions, the transition from *waiting users* to *served users* can be performed by *search & rescue operators* only and is as follows:

$$C_d(t) = \frac{1}{x(t)} \frac{C_0^d z(t)}{B}, \tag{15}$$

where C_0^d is the sidelink downlink capacity, whereas $z(t)$ is the actual number of *search & rescue operators*.

Note: Capacities (in Mbps) for unicast, multicast, and sidelink transmissions can be obtained as:

$$C_o^* = W \log_2(1 + \mathrm{SNR}(d_{3\mathrm{d}})), \tag{16}$$

where W is the available bandwidth in MHz.

As users are activated at arbitrary locations, the data rate between the users and the BS constitutes a random variable whose distribution can be obtained from the distribution of distances, taking into account the upper limit of achievable data rate and parameters related to the signal propagation [35]. In the case of multicasting, the data rate of the group is determined by the user with the worst channel conditions. In the case of sidelink connections, direct links can either perform or not. Therefore, a fixed data rate value is achieved within a fixed distance.

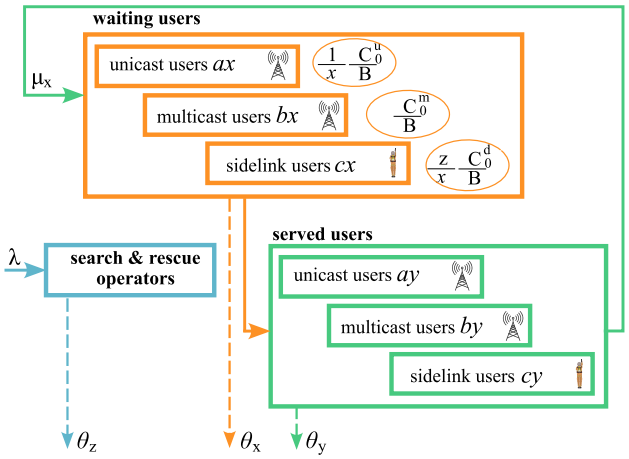

FIGURE 2. Framework illustration.

V. ANALYZING NETWORK TRAFFIC

This section presents our developed fluid approximation for characterizing the number of *waiting users*, *served users*, and *search & rescue operators* (such as policemen, ambulance personnel, and fire brigades) by capturing the time dynamics of arrival/departure/transition processes in their transient phases. *Waiting users* can receive the required content by means of either a unicast, multicast, or sidelink transmission. For a schematic representation of the processes underlying the proposed model, we refer readers to Fig. 2.

Users and *search & rescue operators* are considered as continuous fluids. The number of *waiting users* at time t corresponds to $x(t)$, the number of *served users* at time t is denoted as $y(t)$, whereas we refer to the number of *search & rescue operators* at time t as $z(t)$. We underline that $x(t)$, $y(t)$, and $z(t)$ are any non-negative real numbers, not compulsory integers.

For the sake of simplicity, we omit the index t. The evolution of x, y, and z is then defined by the solution to the Cauchy problem.

In the considered mission-critical situation, *waiting users* and *served users* are assumed to be present in the area of interest, while *search & rescue operators* arrive after an emergency. The formulation of the Cauchy problem in such a scenario to obtain the thought solution is given by

$$\begin{cases} x' = y\mu_x - a\frac{C_0^u}{B} - bx\frac{C_0^m}{B} - cz\frac{C_0^d}{B} - x\theta_x, \\ y' = a\frac{C_0^u}{B} + bx\frac{C_0^m}{B} + cz\frac{C_0^d}{B} - y\theta_y - y\mu_x, \\ z' = \lambda - z\theta_z, \\ \text{under initial conditions:} \\ x(0) = N_x, y(0) = N_y, z(0) = 0, \end{cases} \tag{17}$$

where a, b, and c are weight parameters used to perform resource splitting among transmission modes.

We first define z as

$$z = \frac{\lambda}{\theta_z} + C_z e^{-\theta_z t}, \tag{18}$$

Taking into account initial condition $z(0) = 0$, we obtain C_z:

$$C_z = -\frac{\lambda}{\theta_z}. \tag{19}$$

Therefore, the Cauchy problem (17) can be transformed into:

$$\begin{cases} x' = y\mu_x - a\frac{C_0^u}{B} - bx\frac{C_0^m}{B} - c\frac{C_0^d}{B}\left(\frac{\lambda-\lambda e^{-\theta_z t}}{\theta_z}\right) - x\theta_x, \\ y' = a\frac{C_0^u}{B} + bx\frac{C_0^m}{B} + c\frac{C_0^d}{B}\left(\frac{\lambda-\lambda e^{-\theta_z t}}{\theta_z}\right) - y\theta_y - y\mu_x, \\ \text{under initial conditions:} \\ x(0) = N_x, y(0) = N_y. \end{cases} \tag{20}$$

We then solve the problem at hand by expressing the variable y from the first equation of (20):

$$y = \frac{1}{\mu_x}x' + a\frac{C_0^u}{B} + bx\frac{C_0^m}{B} + c\frac{C_0^d}{B}\left(\frac{\lambda - \lambda e^{-\theta_z t}}{\theta_z}\right) + x\theta_x. \tag{21}$$

We further derive y' from the equation (21) as

$$y' = \frac{1}{\mu_x}\left[x'' + bx'\frac{C_0^m}{B} + x'\theta_x\right]. \tag{22}$$

We substitute the expression derived from equation for y as per (21) and y' as per (22) into the second equation of (20):

$$x'' + x'\left[b\frac{C_0^m}{B} + \theta_x + \theta_y + \mu_x\right] + x\left[b\frac{\theta_y C_0^m}{B} + \theta_x\theta_y + \theta_x\mu_x\right] = \theta_y\left[-a\frac{C_0^u}{B} - c\frac{C_0^d(\lambda - \lambda e^{-\theta_z t})}{\theta_z B}\right]. \tag{23}$$

This means that the characteristic equation of the non-homogeneous differential equation (23) is given by:

$$\mathcal{X}^2 + \left[b\frac{C_0^m}{B} + \theta_x + \theta_y + \mu_x\right]\mathcal{X} + \left[b\frac{\theta_y C_0^m}{B} + \theta_x\theta_y + \theta_x\mu_x\right] = 0. \tag{24}$$

The roots of (24) are as follows:

$$\mathcal{X}_{1,2} = \frac{1}{2}\left[\frac{-bC_0^m}{B} - \theta_x - \theta_y - \mu_x \pm \sqrt{D}\right], \tag{25}$$

where $D = \frac{1}{B^2}[b^2 C_0^{m^2} + 2bBC_0^m(\theta_x - \theta_y + \mu_x) + B^2(\theta_x^2 - 2\theta_x(\mu_x + \theta_y) + \mu_x^2 + 2\mu_x\theta_y + \theta_y^2)]$.

The solution of the non-homogeneous differential equation (23), therefore, is given as:

$$x = C_1 e^{\mathcal{X}_1 t} + C_2 e^{\mathcal{X}_2 t} + A, \tag{26}$$

where A represents the particular solution of the non-homogeneous differential equation (23) and is as follows

$$A = \frac{\left[-a\frac{C_0^u}{B} - c\frac{C_0^d(\lambda - \lambda e^{-\theta_z t})}{\theta_z B}\right]\theta_y}{\left[b\frac{\theta_y C_0^m}{B} + \theta_x\theta_y + \theta_x\mu_x\right]}. \tag{27}$$

Therefore, the corresponding solution to the system (20) for y is given as:

$$y = \frac{1}{\mu_x}\left[\mathcal{X}_1 C_1 e^{\mathcal{X}_1 t} + \mathcal{X}_2 C_2 e^{\mathcal{X}_2 t} + a\frac{C_0^u}{B} + \theta_x\left[C_1 e^{\mathcal{X}_1 t} + C_2 e^{\mathcal{X}_2 t} + A\right] + b\frac{C_0^m}{B}\left[C_1 e^{\mathcal{X}_1 t} + C_2 e^{\mathcal{X}_2 t} + A\right] + c\frac{C_0^d}{B}\left(\frac{\lambda - \lambda e^{-\theta_z t}}{\theta_z}\right)\right]. \tag{28}$$

Taking into account initial conditions $x(0) = N_x$, $y(0) = N_y$, we obtain the following system of equations:

$$\begin{cases} C_1 + C_2 + \frac{\left[-a\frac{C_0^u}{B}\right]\theta_y}{\left[b\frac{\theta_y C_0^m}{B} + \theta_x\theta_y + \theta_x\mu_x\right]} = N_x \\ \frac{1}{\mu_x}\left[b\frac{C_0^m}{B}\left[C_1 + C_2 + \frac{\left[-a\frac{C_0^u}{B}\right]\theta_y}{\left[b\frac{\theta_y C_0^m}{B} + \theta_x\theta_y + \theta_x\mu_x\right]}\right] + \mathcal{X}_1 C_1 + \mathcal{X}_2 C_2\right. \\ \left. + a\frac{C_0^u}{B} + \theta_x\left[C_1 + C_2 + \frac{\left[-a\frac{C_0^u}{B}\right]\theta_y}{\left[b\frac{\theta_y C_0^m}{B} + \theta_x\theta_y + \theta_x\mu_x\right]}\right]\right] = N_y. \end{cases}$$

Therefore, C_1 and C_2 are given as:

$$C_1 = N_x - C_2 - \frac{\left[-a\frac{C_0^u}{B}\right]\theta_y}{\left[b\frac{\theta_y C_0^m}{B} + \theta_x\theta_y + \theta_x\mu_x\right]}, \tag{29}$$

$$C_2 = \frac{1}{(\mathcal{X}_1 - \mathcal{X}_2)}\left[\mathcal{X}_1 N_x - \mathcal{X}_1\frac{\left[-a\frac{C_0^u}{B}\right]\theta_y}{\left[b\frac{\theta_y C_0^m}{B} + \theta_x\theta_y + \theta_x\mu_x\right]} + a\frac{C_0^u}{B} + b\frac{C_0^m}{B}N_x + \theta_x N_x - N_y\mu_x\right]. \tag{30}$$

VI. PERFORMANCE EVALUATION

This section discusses the results obtained from the link-level evaluation of the proposed analytical fluid-based framework for mission-critical scenarios.

In the following, we will first describe the reference scenarios for our performance evaluation campaign and the main simulation parameters implemented in the MATLAB environment. Then, we verify the proposed analytical model through computer simulations and analyze the behavior of the configuration options introduced in Section III.

A. SCENARIOS AND PARAMETERS

In the simulated mission-critical scenario, illustrated in Fig. 1, two IAB nodes are located outdoors. The fixed IAB connects to the 5G NR BS the edge IAB vehicular that serves multiple users existing in the indoor environment. This results in a mixed indoor/outdoor propagation scenario.

Specifically, data is delivered through the following path: 5G NR BS → fixed IAB (UMi) → edge IAB vehicular (UMi) → users (Umi O2I, InH). The area of interest is 500 m x 500 m. The locations of the 5G NR BS and the fixed IAB node are at coordinates $(0, 0, 10)$ and $(100, 100, 10)$, respectively.

The distribution of the users inside the building is dependent on a reference point representing the center of the building, which is uniformly distributed around the area of interest. Users are uniformly distributed around the reference point within a radius of 20 m. In order to establish a reliable connection, the edge IAB vehicle location is adjusted to the building location at 50 m distance from the reference point.

Regarding the access connection, all options (i.e., unicast, multicast, sidelink, and mixed modes) discussed in Section V are analyzed. Our system operates within the 5G frequency range 2 (FR2). We use MATLAB Antenna Toolbox to model antenna directivity patterns for uniform rectangular arrays with isotropic elements, Chebyshev tapering, and no steering. We assume the fixed transmit power of 23 dBm coming from the BS and IABs, while the transmit power at users is set to 10 dBm. We assume the SNR threshold of -9.478 dB at the receiver side, corresponding to the lowest modulation and coding scheme (MCS 0).

We note that *waiting users* can change their state to *served users* after receiving a video with instructions on how to proceed within the emergency scenario. We assume a video duration of 30 seconds, with a resolution of 1280x720 pixels and H.264 encoding, resulting in a content size of 80 MB.

We evaluate the following exemplary scenarios:

- *Scenario 1.* We assume that *search & rescue operators* arrive in the system with a rate of $\lambda_z = 5.5$ during time interval $(0, t]$, while *waiting users* and *served users* do not arrive to the system. At the time the critical event occurs ($t = 0$), we assume that $N_x = 30$ *waiting users* and $N_y = 0$ *served users* are in the area of interest. *Waiting users* and *served users* cannot leave the system that is the departure rates $\theta_x = 0$ and $\theta_y = 0$, respectively. *Search & rescue operators* may leave the system with the rate $\theta_z = 0.1$. The transition from *served user* to *waiting user* cannot happen, i.e., $\mu_x = 0$.
- *Scenario 2.* Differently from the one previously described, in this scenario *waiting users* and *served users* may leave the system. In addition, *served users* may transit back to *waiting users* due to content loss or the need for additional instructions. The departure rates are defined as $\theta_x = 0.2$ for *waiting users* and $\theta_y = 0.7$ for *served users*. This means that *served users* are more likely to leave the system since they receive instructions on how to behave in an emergency situation. The transition from *served user* to *waiting user* can be performed with $\mu_x = 0.4$.
- *Scenario 3.* We test a situation where the departure rate for *waiting users* is set to $\theta_x = 0$, indicating that no *waiting users* are able to leave the system, i.e., users may leave the system only after receiving the content. The departure rate for *served users* is defined as $\theta_y = 0.7$. This scenario introduces additional complexity as it requires sending instructions multiple times, resulting in the transition from *served users* to *waiting users* occurring at a rate of $\mu_x = 0.9$. The rest of the settings is based on Scenario 1.

We provide the results in terms of the following metrics:

- number of *waiting users*, *served users*, and *search & rescue operators*;
- delivered content size [Gbit], calculated as the total amount of bits delivered to the users (by means of unicast, multicast, and/or sidelink transmissions);
- actual data rate [Gbits] for unicast, multicast, and/or sidelink transmissions.

Modeling parameters adopted in the simulations are reported in Table 3.

B. UNDERSTANDING ANALYTICAL RESULTS

We recall that we aim to analyze mission-critical and emergency situations characterized by system operation in its temporary phase. For this reason, we consider the evolution of users requesting service within the content lifetime. Importantly, we cannot invoke the system's functioning in a steady state (i.e., unchanged across time) since the content lifespan cannot be considered long enough to achieve the stationary state.

We start by validating the proposed analytical framework (A) through computer simulations (S) for Scenario 1. Table 4 provides insights into the time required to serve all users depending on the configuration option (i.e., standalone transmission or mixed modes) and under different resource sharing ratios. The first aspect we wish to highlight is the close match observed between simulation results and analytical results. This assessment confirms the applicability of the proposed method in capturing the time dynamics of mission-critical services, particularly during the non-static transient phase.

First, we compare configurations 1-3, which represent different standalone modes of operation, i.e., unicast, multicast, and sidelink modes, which exhibit service times of 34.9, 10.3, and 11.3 seconds, respectively. These results can be explained by the fact that users inside the building are situated close to each other. Thus, one multicast transmission can cover them with a relatively strong link. We recall that multicast directional communications are characterized by wider beams compared to unicast and sidelink ones. Differently, simultaneous unicast transmissions share the power budget of the antenna, whereas sidelink transmissions are usually performed in proximity with reduced transmit power due to the hardware on the devices.

However, it is important to note that one technology alone may not always guarantee the best performance. For example, while multicasting can be more efficient in serving users located in close proximity to each other, there may

TABLE 3. Simulation parameters.

Parameter	Value
Area	500 m x 500 m
Carrier frequency, f_c	28 GHz (FR 2)
Total bandwidth	100 MHz
Height of BS/IAB fixed, h_T	10 m (UMi) [32]
Height of UEs, h_u	1.5 m [32]
Height of edge IAB vehicular	1.5 m
Number of BSs	1 BS
SNR threshold	-9.478 dB
Transmit power	23 dBm [BS]/ 10 dBm [UE] [36]
Distance between edge IAB vehicular and reference point, d	50 m
Fading margin	4 dB
Interference margin	3 dB
Antenna array	64x64,32x32,16x16,8x8,4x4,2x2
Maximum radius between sidelink users, R	20 m
Packet size, B	80 MB (30 seconds video with resolution of 1280x720 pixels and H.264 encoding)
Arrival rate of search & rescue operators, λ	5.5 s^{-1}
Departure rate of waiting users, θ_x	vary
Departure rate of served users, θ_y	vary
Departure rate of search & rescue operators	vary
Transition rate from served users to waiting users	vary

TABLE 4. Time required to serve all users (Scenario 1).

Configuration option	Resource sharing ratio, %	Time, s (S/A)
1: Unicast mode	100	34.82/34.82
2: Multicast mode	100	14.29/14.29
3: Sidelink mode	100	11.22/11.22
4: Mixed Unicast-Multicast mode	10/90	6.28/6.28
	20/80	**6.08/6.08**
	30/70	6.20/6.20
	50/50	7.05/7.05
	70/30	9.10/9.10
	80/20	11.22/11.22
	90/10	15.67/15.67
5: Mixed Unicast-Sidelink mode	**10/90**	**11.70/11.70**
	20/80	12.27/12.27
	30/70	12.94/12.94
	50/50	14.77/14.77
	70/30	17.88/17.88
	80/20	20.54/20.54
	90/10	25.01/25.01
6: Mixed Multicast-Sidelink mode	10/90	8.51/8.51
	20/80	7.16/7.16
	30/70	6.34/6.34
	50/50	5.40/5.40
	70/30	**5.10/5.10**
	80/20	**5.09/5.09**
	90/10	5.23/5.23
7: Mixed Unicast-Multicast-Sidelink mode	10/10/80	8.79/8.79
	20/20/60	7.62/7.62
	33/33/33	6.92/6.92
	10/80/10	5.36/5.36
	5/80/15	**5.15/5.15**
	1/80/19	**5.02/5.02**
	20/60/20	5.59/5.59
	80/10/10	13.43/13.43
	60/20/20	9.23/9.23

be scenarios where unicast and sidelink transmissions are necessary to ensure optimal performance. Therefore, the possibility to combine multicasting, unicast, and sidelink operations needs to be considered in case this allows to achieve fast and efficient transmissions, taking into account the specific characteristics and requirements of the users and their locations.

In this vein, we also analyze mixed configurations, starting with those involving two technologies (Configurations 4, 5, and 6). In general, we can state that the distribution of resources among transmission modes significantly impacts the overall time required to serve users. Specifically, Configuration 4 (Mixed Unicast-Multicast mode) demonstrates that the service time decreases as the resource sharing ratio shifts towards multicasting. The lowest service time is 6.08 seconds at 20%/80% resource sharing ratio (multicast occupies 80% of the total 100% resources). Configuration 5 (Mixed Unicast-Sidelink mode) exhibits a similar trend when the sidelink technology is coupled with multicasting. The lowest time achieved corresponds to 11.7 seconds at 10%/90% resource sharing, and as the resource sharing ratio shifts towards sidelink, the time gradually increases. Configuration 6 (Mixed Multicast-Sidelink mode) shows that the lowest time is achieved at 70%/30% resource sharing, corresponding to 5.09 seconds. Thus, we can infer that the interplay of two technologies facilitates the efficient offloading of traffic from the "partner" mode.

Finally, we consider the combined exploitation of all considered technologies by analyzing Configuration 7 (Mixed Unicast-Multicast-Sidelink mode), demonstrating a more complex relationship between resource sharing ratios and service time. The lowest service time is achieved at 5%/80%/15% resource sharing ratio, resulting in a time of 5.15 seconds, with a slight improvement at 1%/80%/19% resource sharing ratio of 0.13 seconds. Based on these comparisons, one may note that the most efficient configuration in terms of service time depends on the specific resource sharing ratios and modes. However, considering the lowest times achieved in the given table, Configuration 7 shows the best overall performance, making it the preferred solution for mission-critical services. Furthermore, the observed trends in the results validate the following findings. The utilization of multicasting in combination with unicast and sidelink transmissions demonstrates its ability to facilitate efficient content delivery. The system exhibits improved performance when a higher proportion of multicast resources is allocated compared to unicast and sidelink resources. This highlights the advantage of *prioritizing multicast to enhance overall system efficiency and optimize content dissemination*. Thus, for the above-discussed reasons, from now on, we concentrate on Configuration 7 only.

In Fig. 3, we show results in terms of the metrics of interest achieved in Scenario 1 with 1/%80/%19% resource sharing ratio. We point out that the slope of the green curves (representing *served users*) in subfigures (a) and (b) indicates the speed at which users acquire the content. Specifically, the steeper the slope upward in subfigures (a) and (b) (i.e., the higher the value), the better. Moreover, a considerable difference between green and orange curves (*served* and *waiting users*) in subfigures (a) shows fast delivery speed and fewer users waiting to be served. The results confirm that for the considered settings and input parameters, the mix of the three transmission modes guarantees a fast content dissemination due to the ability to capture the channel conditions of

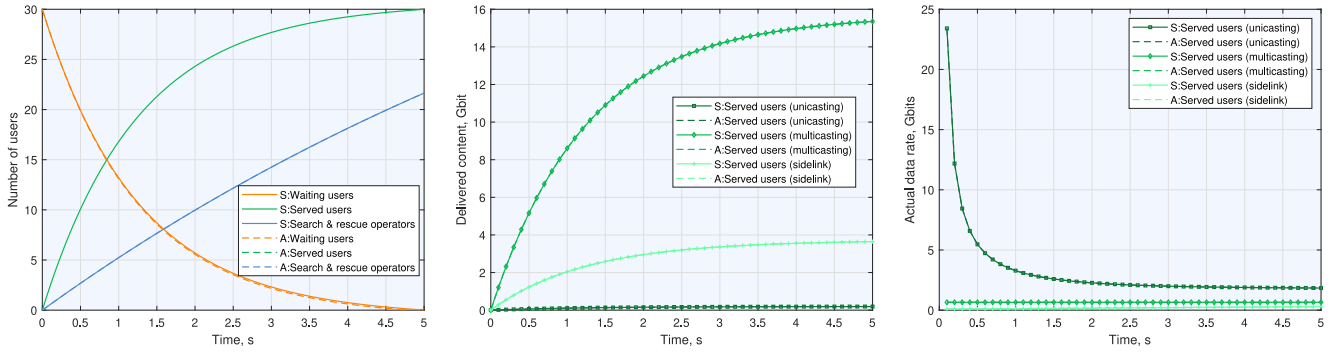

(a) Number of nodes (b) Delivered content (c) Data rate

FIGURE 3. Scenario 1: Performance assessment of Configuration 7 (Mixed Unicast-Multicast-Sidelink mode), $a = 0.01$, $b = 0.8$, and $c = 0.19$.

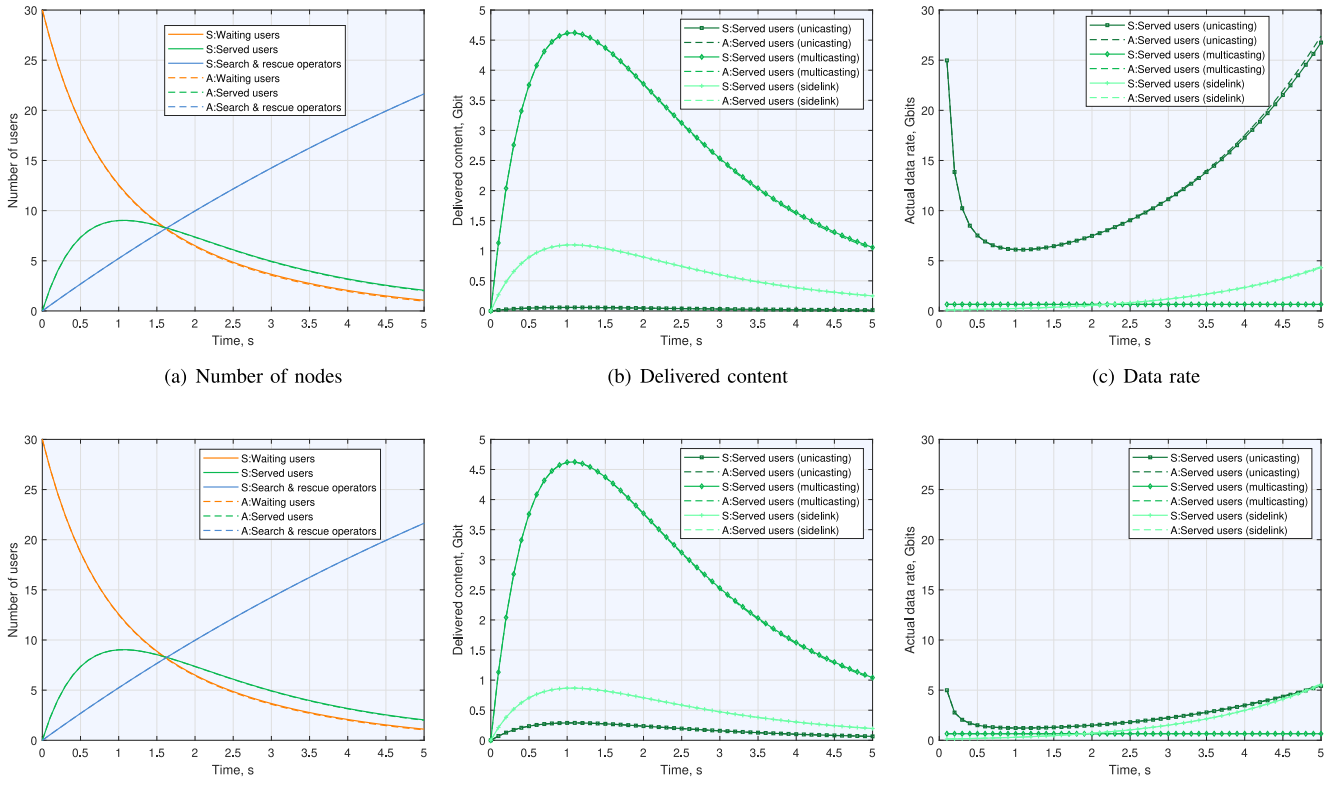

(a) Number of nodes (b) Delivered content (c) Data rate

(d) Number of nodes (e) Delivered content (f) Data rate

FIGURE 4. Scenario 2: Performance assessment of Configuration 7 (Mixed Unicast-Multicast-Sidelink mode), $a = 0.01$, $b = 0.8$, and $c = 0.19$ ((a), (b), and (c)), $a = 0.05$, $b = 0.8$, and $c = 0.15$ ((d), (e), and (f)).

users, thus assuring mission-critical service delivery without considerable delay, which is essential in the case of disasters.

We then proceed to investigate Scenario 2 for Configuration 7 in Fig. 4 for 1%/80%/19% and 5%/80%/15% resource sharing ratios, respectively. The trend of the curves in all subfigures differs from Scenario 1 due to different input parameters. Since *waiting users* and *served users* have the possibility to leave the system and/or change their state, the number of *served users* and the delivered content will not continuously increase as in Fig. 4, but will change over time. Initially, they will grow at a lower rate w.r.t. Scenario 1 and then slowly decrease due to the joint effect of state transition and departure process of both waiting and served users. The trend for the unicast data rate (see Fig. 4(c) and (f)) is the opposite: it initially drops as the number of users grows and then gradually increases because of the reduction in the number of users in the system and, consequently, of the more likely establishment of unicast transmissions due to users' sparsity. It is important to highlight that the unicast data rate in case of lower resource ratio assigned to unicasting (see the dark green curve in Fig. 4(c) w.r.t. (f)) is higher due to the lower number of simultaneous unicast transmissions, leading to higher per-transmission power. On the other hand, the sidelink data rate shows a

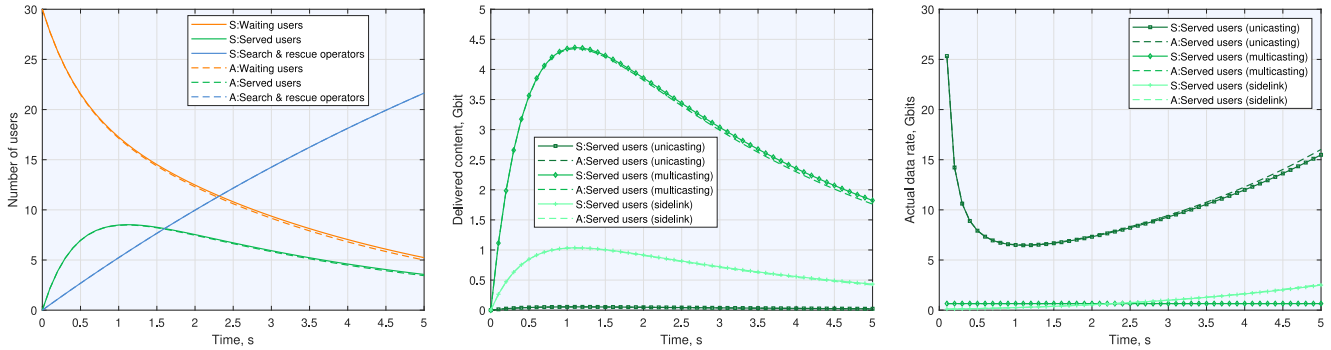

(a) Number of nodes (b) Delivered content (c) Data rate

FIGURE 5. Scenario 3: Performance assessment of Configuration 7 (Mixed Unicast-Multicast-Sidelink mode), $a = 0.05$, $b = 0.8$, and $c = 0.15$.

constant growth, as the number of search & rescue operators (see blue curve in Fig. 4(a) and (d)), while the multicast data rate remains constant throughout the emergency situation.

Fig. 5 shows that in Scenario 3, there is a slower decrease in the number of *waiting users* compared to Scenario 2. This is because *waiting users* cannot leave the system without receiving the instructions. In this case, the number of *waiting users* can only decrease when they change their state to *served users*. Similarly, the number of *served users* decreases at a lower rate due to the possibility of acquiring the content multiple times. These factors impact both the amount of delivered content and the data rate values.

In conclusion, our analysis and simulations have demonstrated the effectiveness of a mixed transmission approach combining unicast, multicast, and sidelink modes for mission-critical service delivery. While standalone modes can be efficient in certain scenarios, a combination of these technologies is necessary to ensure fast and efficient content dissemination, considering the specific characteristics and requirements of the users and their locations.

VII. CONCLUSION AND FUTURE WORK

This article has analyzed a mission-critical situation in which the BS is temporarily unavailable or unreachable, and the network topology is enhanced by IAB nodes.

We have focused on the processes that tend to be in the non-static transient phase, usually referred to as short-term operating time intervals that occur in the transition between various steady-state conditions (constant or unchanged across time). Transient analysis, by definition, includes time-varying loads, i.e., loads that are a function of time, and depends on arrival, transition, and departure processes. The general forms for such processes are presented in systems of equations as per (17), and include the topological randomness of user deployment, assuming that user coordinates are random variables that may be parameterized in reality by a mobility pattern.

In such a scenario, we have investigated the interplay of sidelink communications, directional unicast transmissions, and multicasting. Notably, this study combines a mathematical model for analyzing network configuration options for mission-critical communications with extensive link-level simulations. We have deduced from the findings that the proposed model allows the emergency management team to select the network configuration that best fits the mission-critical circumstance under control. The model also guarantees exemplary functional connectivity in emergencies, which is critical for successful public protection and disaster relief efforts.

Specifically, among the technologies examined, multicasting consistently emerged as an efficient solution in all configuration options. Given the same settings and input parameters, multicast facilitates unicast and sidelink transmissions by delivering the content more efficiently. Allocating a higher proportion of multicast resources compared to unicast and sidelink resources resulted in improved system performance. This emphasizes the advantage of prioritizing multicast to enhance system efficiency and optimize content dissemination.

Looking ahead, aligning with the trends in 6G-oriented technology to ensure functional connectivity in emergencies is crucial. Reconfigurable Intelligent Surfaces (RIS) [37], [38], ubiquitous connectivity, integrated sensing and communication (ISAC), and integrated artificial intelligence (AI) and communications are expected to play a critical role [39] and could potentially be integrated into 5G-Advanced and beyond. These advancements, in conjunction with the IAB feature and the interplay of sidelink communications, directional unicast transmissions, and multicasting, have the potential to revolutionize mission-critical communications in the 6G era. This holds promise for enhancing system efficiency, optimizing content dissemination, and enabling successful public protection and disaster relief efforts in the future.

Reproducible Research: The open-source code is available from https://github.com/OlgaChukhno/.

REFERENCES

[1] J. Li et al., "5G new radio for public safety mission critical communications," *IEEE Commun. Stand. Mag.*, vol. 6, no. 4, pp. 48–55, Dec. 2022.

[2] M. Condoluci, G. Araniti, T. Mahmoodi, and M. Dohler, "Enabling the IoT machine age with 5G: Machine-type multicast services for innovative real-time applications," *IEEE Access*, vol. 4, pp. 5555–5569, 2016.

[3] "Mission critical services in 3GPP." 3GPP. 2017. [Online]. Available: https://www.3gpp.org/news-events/3gpp-news/mc-services

[4] A. Kumbhar, F. Koohifar, I. Güvenç, and B. Mueller, "A survey on legacy and emerging technologies for public safety communications," *IEEE Commun. Surveys Tuts.*, vol. 19, no. 1, pp. 97–124, 1st Quart., 2017.

[5] H. Ronkainen, J. Edstam, A. Ericsson, and C. Östberg, *Integrated Access and Backhaul—A New Type of Wireless Backhaul in 5G: Ericsson Technology Review*, Ericsson, Stockholm, Sweden, pp. 2–11, 2020.

[6] H. Holma, A. Toskala, and T. Nakamura, *5G Technology: 3GPP New Radio*. Hoboken, NJ, USA: Wiley, 2020.

[7] V. Petrov et al., "Achieving end-to-end reliability of mission-critical traffic in softwarized 5G networks," *IEEE J. Sel. Areas Commun.*, vol. 36, no. 3, pp. 485–501, Mar. 2018.

[8] D. Yu, W. Li, H. Xu, and L. Zhang, "Low reliable and low latency communications for mission critical distributed Industrial Internet of Things," *IEEE Commun. Lett.*, vol. 25, no. 1, pp. 313–317, Jan. 2021.

[9] V. K. Lau, S. Cai, and M. Yu, "Decentralized state-driven multiple access and information fusion of mission-critical IoT sensors for 5G wireless networks," *IEEE J. Sel. Areas Commun.*, vol. 38, no. 5, pp. 869–884, May 2020.

[10] M. Tang, S. Cai, and V. K. N. Lau, "Remote state estimation with asynchronous mission-critical IoT sensors," *IEEE J. Sel. Areas Commun.*, vol. 39, no. 3, pp. 835–850, Mar. 2021.

[11] S. Saafi, J. Hosek, and A. Kolackova, "Enabling next-generation public safety operations with mission-critical networks and wearable applications," *Sensors*, vol. 21, no. 17, p. 5790, 2021.

[12] A. Orsino et al., "Effects of heterogeneous mobility on D2D- and drone-assisted mission-critical MTC in 5G," *IEEE Commun. Mag.*, vol. 55, no. 2, pp. 79–87, Feb. 2017.

[13] A. Orsino et al., "Exploiting D2D communications at the network edge for mission-critical IoT applications," in *Proc. 23rd Eur. Wireless Conf. Eur. Wireless*, 2017, pp. 1–6.

[14] D. Wang, H. Qin, B. Song, K. Xu, X. Du, and M. Guizani, "Joint resource allocation and power control for D2D communication with deep reinforcement learning in MCC," *Phys. Commun.*, vol. 45, Apr. 2021, Art. no. 101262.

[15] A. Elshrkasi, K. Dimyati, K. A. B. Ahmad, and M. F. B. M. Said, "Enhancement of cellular networks via an improved clustering technique with D2D communication for mission-critical applications," *J. Netw. Comput. Appl.*, vol. 206, Oct. 2022, Art. no. 103482.

[16] P. K. Sharma, P. Raut, T. A. Tsiftsis, and P. Peshwe, "Cognitive D2D finite blocklength transmissions with the presence of time-selective interference," *IEEE Trans. Veh. Technol.*, vol. 70, no. 11, pp. 12215–12219, Nov. 2021.

[17] N. Chukhno, A. Orsino, J. Torsner, A. Iera, and G. Araniti, "5G NR sidelink multi-hop transmission in public safety and factory automation scenarios," *IEEE Netw.*, early access, Jan. 16, 2023, doi: 10.1109/MNET.124.2100765.

[18] A. Daher, M. Coupechoux, P. Godlewski, J.-M. Kelif, P. Ngouat, and P. Minot, "SINR model for MBSFN based mission critical communications," in *Proc. IEEE 86th Veh. Technol. Conf. (VTC-Fall)*, 2017, pp. 1–5.

[19] D. Jagyasi, M. Coupechoux, and A. Daher, "Multi-cell MIMO transceiver design for mission-critical communication," in *Proc. IEEE Global Commun. Conf. (GLOBECOM)*, 2019, pp. 1–6.

[20] A. Daher, M. Coupechoux, P. Godlewski, P. Ngouat, and P. Minot, "A dynamic clustering algorithm for multi-point transmissions in mission-critical communications," *IEEE Trans. Wireless Commun.*, vol. 19, no. 7, pp. 4934–4946, Jul. 2020.

[21] J. Vargas, C. Thienot, and X. Lagrange, "Comparison of MBSFN, SC-PTM and unicast for mission critical communication," in *Proc. 24th Int. Symp. Wireless Pers. Multimedia Commun. (WPMC)*, 2021, pp. 1–6.

[22] M. Polese et al., "Integrated access and backhaul in 5G mmWave networks: Potential and challenges," *IEEE Commun. Mag.*, vol. 58, no. 3, pp. 62–68, Mar. 2020.

[23] N. Tafintsev et al., "Aerial access and backhaul in mmWave B5G systems: Performance dynamics and optimization," *IEEE Commun. Mag.*, vol. 58, no. 2, pp. 93–99, Feb. 2020.

[24] H. Zhang et al., "Autonomous navigation and configuration of integrated access backhauling for UAV base station using reinforcement learning," in *Proc. IEEE Future Netw. World Forum (FNWF)*, 2022, pp. 184–189.

[25] A. Merwaday, A. Tuncer, A. Kumbhar, and I. Guvenc, "Improved throughput coverage in natural disasters: Unmanned aerial base stations for public-safety communications," *IEEE Veh. Technol. Mag.*, vol. 11, no. 4, pp. 53–60, Dec. 2016.

[26] S. A. R. Naqvi, S. A. Hassan, H. Pervaiz, and Q. Ni, "Drone-aided communication as a key enabler for 5G and resilient public safety networks," *IEEE Commun. Mag.*, vol. 56, no. 1, pp. 36–42, Jan. 2018.

[27] C. Madapatha, B. Makki, A. Muhammad, E. Dahlman, M.-S. Alouini, and T. Svensson, "On topology optimization and routing in integrated access and backhaul networks: A genetic algorithm-based approach," *IEEE Open J. Commun. Soc.*, vol. 2, pp. 2273–2291, 2021.

[28] "Becoming 5G advanced: The 3GPP 2025 Roadmap." 5G Americas. 2022. [Online]. Available: https://www.5gamericas.org/wp-content/uploads/2022/12/Becoming-5G-Advanced-the-3GPP-2025-Roadmap-InDesign.pdf

[29] "Study on channel model for frequencies from 0.5 to 100 GHz (Release 17)," 3GPP, Sophia Antipolis, France, Rep. TR 38.901, Version 17.0.0, Mar. 2022.

[30] R. J. Weiler, M. Peter, W. Keusgen, K. Sakaguchi, and F. Undi, "Environment induced shadowing of urban millimeter-wave access links," *IEEE Wireless Commun. Lett.*, vol. 5, no. 4, pp. 440–443, Aug. 2016.

[31] G. R. MacCartney, T. S. Rappaport, and S. Rangan, "Rapid fading due to human blockage in pedestrian crowds at 5G millimeter-wave frequencies," in *Proc. IEEE Global Commun. Conf.*, 2017, pp. 1–7.

[32] "Technical specification group radio access network; study on channel model for frequency spectrum above 6 GHz (Release 15)," 3GPP, Sophia Antipolis, France, Rep. TR 38.900, Version 15.0.0, Jun. 2018.

[33] O. Chukhno, N. Chukhno, O. Galinina, Y. Gaidamaka, S. Andreev, and K. Samouylov, "Analysis of 3D deafness effects in highly directional mmWave communications," in *Proc. IEEE Global Commun. Conf. (GLOBECOM)*, 2019, pp. 1–6.

[34] O. Chukhno et al., "A holistic assessment of directional deafness in mmWave-based distributed 3D networks," *IEEE Trans. Wireless Commun.*, vol. 21, no. 9, pp. 7491–7505, Sep. 2022.

[35] O. Galinina, A. Pyattaev, K. Johnsson, S. Andreev, and Y. Koucheryavy, "Analyzing effects of directional deafness on mmWave channel access in unlicensed bands," in *Proc. IEEE Globecom Workshops (GC Wkshps)*, 2017, pp. 1–7.

[36] *Study on LTE Device to Device Proximity Services; Radio Aspects (Release 12)*, 3GPP Standard TS 36.843, Version 12.0.1, Mar. 2014.

[37] R. Liu, Q. Wu, M. Renzo, and Y. Yuan, "A path to smart radio environments: An industrial viewpoint on reconfigurable intelligent surfaces," *IEEE Wireless Commun.*, vol. 29, no. 1, pp. 202–208, Feb. 2022.

[38] R. Liu, J. Dou, P. Li, J. Wu, and Y. Cui, "Simulation and field trial results of reconfigurable intelligent surfaces in 5G networks," *IEEE Access*, vol. 10, pp. 122786–122795, 2022.

[39] R. Liu, R. Y.-N. Li, M. D. Renzo, and L. Hanzo, "A vision and an evolutionary framework for 6G: Scenarios, capabilities and enablers," 2023, *arXiv:2305.13887*.